Progress in Natural Science: Materials International 2013;23(4):395–401

Chinese Materials Research Society

Progress in Natural Science: Materials International

www.elsevier.com/locate/pnsmi
www.sciencedirect.com

ORIGINAL RESEARCH

Novel electric conductive polylactide/carbon nanotubes foams prepared by supercritical CO_2

Ting He, Xia Liao*, Yunchuan He, Guangxian Li**

College of Polymer Science and Engineering, State Key Laboratory of Polymer Materials Engineering, Sichuan University, Chengdu 610065, Sichuan, China

Received 5 November 2012; accepted 6 May 2013
Available online 19 July 2013

KEYWORDS

Supercritical CO_2;
Polylactide;
Multiwall carbon nanotubes;
Electric conductive foam;
Nanocomposite

Abstract In this paper, novel electric conductive polylactide/carbon nanotubes (PLA/CNTs) foams were fabricated by a pressure-quench process using supercritical CO_2 as a blowing agent. The morphology of PLA/CNTs nanocomposites prepared by solution blending was characterized using SEM and the results indicate that CNTs well dispersed in PLA matrix. The introduction of CNTs improved the thermal stability of PLA. The morphology and electrical properties of PLA/CNTs foams were characterized and discussed. Depending on the process parameters, such as saturation temperature and pressure, nanocellular or microcellular structure of PLA/CNTs nanocomposites were obtained. The volume resistivity of PLA/CNTs foams was from 0.53×10^3 Ω cm to 15.13×10^3 Ω cm, which was affected by cell structure and crystallization of foams oppositely. Foaming reduced the electrical conductivity due to the decrease of CNTs volume content and the break of conductive pathways. However, crystallization increased the electrical conductivity possibly because of the CNTs structural change in which the CNTs were less curled and more connected.

1. Introduction

Polylactide (PLA), produced from renewable resources, has attracted increasingly attention over the past couple decades [1]. It can be an alternative to petroleum-based polymer. The attributes of biodegradability, biocompatibility, good mechanical properties, and versatile fabrication processes make it a promising material for wide applications such as biomedical materials [2,3], textile [4], packing and containers [5,6]. However, PLA is an inherent electrical insulator material, which limits it utilization in electronic

*Corresponding author. Tel.: +86 28 8540 8361.
**Corresponding author. Tel.: +86 28 8546 9011.
E-mail addresses: xliao@scu.edu.cn (X. Liao), guangxianli@scu.edu.cn (G. Li).

Peer review under responsibility of Chinese Materials Research Society.

ELSEVIER Production and hosting by Elsevier

http://dx.doi.org/10.1016/j.pnsc.2013.06.006

parts and electronic packing and containers. Because the static charge easily builds up on such insulator parts by contact, electrical insulator materials possibly produce an electrostatic discharge that may damage sensitive semiconductor devices and interfere with circuit operation.

To solve the problem of electrostatic discharge, an effective method is compounding PLA with electric conductive fillers to form conductive polymer composites (CPC). For electric conductive fillers, such as metal particles and filaments [7,8], carbon particles [9,10], and carbon fibers [11], the electrical conductivity of CPC increases with increasing filler concentration. However, the maximum filler loading is limited because much high loading filler results in the poor mechanical properties [12]. For materials and process cost saving and good mechanical properties, the attainment of a high electrical conductivity at low filler loading is desired. As compared to conventional metal particles and carbon filler, carbon nanotubes (CNTs) have remarkable structural, mechanical and electrical properties, such as smaller diameters, larger aspect ratios, and much higher conductivity and strength [13,14]. With the special nanostructure, CNTs can form conductive network easily at low loading to provide the desired electrical properties [15–18].

A reduction in weight of CPC is of great significance for electronic devices and electronic packing, because it leads to savings in materials and energy and easier manipulation of devices [19]. CPC-based foams are usually an effective way to reduce the weight or density of materials and have many other advantages, such as varied structure design, good chemical stability, easy tuning of electrical conductivity over a wide range, and higher impact strength for packing which protects electronic devices. However, conventional foam production processes produce cells with average size larger than 100 μm in diameter which leads to poor mechanical properties for foam. In addition, big cells with thin walls limit the formation of an effectively conductive network which is one of key factors for conductivity of CPC.

Microcellular foams are defined as foams with cell diameter lower than 10 μm and cell density greater than 10^{10} cells/cm^3 [20]. In general, the microcellular foaming technology uses supercritical fluid (SCF) especially supercritical carbon dioxide ($scCO_2$), instead of chlorofluorocarbons (CFCs) and hydrochlorofluorocarbons (HCFCs) used in traditional foaming which deplete atmospheric ozone, as the blowing agent. Therefore, microcellular foaming technology is friendly for environment. In addition, the tiny size and uniform distribution of the cells make microcellular foams possess properties of high impact strength, high toughness, and high stiffness-to-weight ratio.

A small number of well-dispersed nano-fillers including CNTs in polymer may act as nucleation sites to facilitate the cell nucleation during foaming. Nano-fillers can also improve the viscosity of polymer matrix that is good for foaming of PLA because it can prevent cell coalescing and collapsing during cell growth. Pilla et al. [21] investigated microcellular PLA/CNTs nanocomposites fabricated by microcellular injection molding. The introduction of multiwall carbon nanotubes (MWNTs) in the composites produced a much finer cell structure than neat PLA because MWNTs acted as nucleating agents to cause more cell nucleation and increased the PLA viscosity through inducing a strain hardening behavior to prevent cell growing. Rizvi et al. [22] fabricated solid and porous PLA/MWNTs nanocomposites by melting blending and subsequent batch processing for porous structures. The porous PLA/MWNTs composites containing 2 and 5 wt% MWNTs had lower relative densities, which was attributed to the higher viscosity of the composites suppressing collapse of the cell structure during foaming. A continuous conductive network structure formed in PLA when the concentration of MWNTs was increased from 0.5 wt% to 1 wt%.

Several studies focus on electrically conductive properties of PLA/CNTs nanocomposites and cell structure morphology of foams [21,22]. However, to our knowledge, no research has examined the electrically conductive properties of PLA/CNTs nanocomposite foam and discussed the effect of foam morphology on electrically conductive properties of PLA/CNTs nanocomposite foam. In this study, PLA/CNTs nanocomposites were prepared by solution blending and its electric conductive foams were fabricated by a pressure-quench process using $scCO_2$ as a blowing agent. Morphological, thermal and electrical properties of the nanocomposites and foams were characterized and the effects of cell structure and crystallization on the electrical property of foams are discussed.

2. Experimental

2.1. Materials

PLA (Ingeo™, 2002D) pellets were provided by Natureworks LLC, USA. According to the supplier, its D-isomer content is 4.3%, density is 1.24 g/cm^3 and melt flow rate is 5–7 g/10 min. MWNTs (Timestub™, TNMH5) functionalized with 1.76 wt% hydroxyl groups (–OH) were purchased from Chengdu Organic Chemical Co. Ltd., Chinese Academy of Science. The MWNTs with a purity of 95% have an average outer diameter ranging from 20 to 30 nm and an average length ranging from 10 to 30 μm. CO_2 with a purity of 99.5% was used as the physical blowing agent.

2.2. Preparation of the PLA/CNTs nanocomposites

PLA/CNTs nanocomposites were prepared by a convenient solution process. In brief, PLA was first dissolved in dichloromethane for a few hours till the uniform solution formed. The exact amount of CNTs was dispersed in dichloromethane with continuous mild sonication (360 W) in ice-water bath for 1 h. Then the PLA solution was added to CNTs suspension to obtain PLA/CNTs suspension with the CNTs-to-PLA/CNTs weight ratio of 1 wt%, 2 wt%, 4 wt%. The PLA/CNTs suspension was further sonicated and stirred for 2 h. The resulting suspension was poured into the glass dish and subsequently left to dry for 12 h at room temperature. The resulting film was dried in vacuum oven at 70 °C for 3 days to guarantee the residual solvent evaporating completely. The PLA/CNTs were molded by compression at 190 °C into sheets with thickness of 600 μm, and then quickly quenched in ice water. The PLA/CNTs sheets were cut into 12 × 12 mm^2 for foaming. For comparison, pure PLA samples were obtained under the same solution fabrication process.

2.3. Preparation of PLA/CNTs foam by supercritical CO_2

The PLA/CNTs and PLA foams were prepared with a pressure-quench method described by Goel and Beckman earlier [23]. The sheets samples were enclosed by a high-pressure vessel preheated to the experimental temperature. Then the vessel was pressurized to the desired pressure after flushed with low pressure CO_2 for 3 min. After saturated for 4 h to ensure the equilibrium sorption of the CO_2, the samples underwent a rapid quench of pressure within 3 s for cell nucleation and growth. Subsequently, the samples were taken out from the vessel and cooled down in air for characterization.

2.4. *Characterization*

The dispersion of MWNTs in PLA/CNTs nanocomposites and the cell morphology of the nanocomposites foams were characterized on a Jeol SEM (model JSM 5900LV, Tokyo, Japan). Scanning electron microscopes (SEM) imaging samples were prepared by cryo-fracturing them in liquid nitrogen. Thermal gravimetric analysis (TGA) of the nanocomposites and neat PLA was performed by using a Netzsch 209F1 thermogravimetric analyzer. Samples of about 10 mg were heated from room temperature to 500 °C with a heating rate of 20 °C/min in a nitrogen atmosphere.

Samples weighing 4–6 mg were used for differential scanning calorimetry (DSC) experiments. All the samples were tested by using a differential scanning calorimeter (Q20, TA Instruments) at a heating rate of 10 °C/min in a nitrogen atmosphere from 30 to 190 °C. The degree of crystallinity (χ_c) for composites was calculated by $[(\Delta H_m - \Delta H_c)/\Delta H_f \Phi] \times 100\%$ [24], where ΔH_c is the enthalpy of crystallization and ΔH_m is the enthalpy of melting on heating; the ΔH_f is the theoretical heat of fusion of 100% crystalline PLA with a value of 93 J/g [25]; and Φ is the content of PLA in the nanocomposites.

For electrical conductivity measurements, copper sheets were stuck to the surface of each sample to ensure good contact of the sample surface with the electrodes. Then the volume electrical resistivity was measured using a TH2683 high resistivity meter.

3. Results and discussion

3.1. *Morphology and thermal stability of nanocomposites*

SEM images of PLA/CNTs nanocomposites are shown in Fig. 1. For samples identification purpose, PLA/CNTs nanocomposites with MWNTs content of 1, 2, 4 wt% will be referred to as PLA/CNT1, PLA/CNT2, PLA/CNT4 respectively. There is insignificant change on the fracture surface of nanocomposites with the increasing MWNTs content. A lot of MWNTs exist in PLA matrix as individual fibers and a small number of micro-scale sized aggregates are observed revealing uniform MWNTs dispersion in the PLA matrix.

TGA was carried out to investigate the effect of MWNTs on the thermal stability of PLA in nitrogen environment and the resulting curves are shown in Fig. 2. The onsets degradation temperature (T_d(onset)) of neat PLA is 274 °C. The T_d(onset) of PLA/CNT1, PLA/CNT2, PLA/CNT4 is 333 °C, 330 °C and 334 °C, respectively. The T_d(onset) for PLA/CNTs nanocomposites is much higher than that for neat PLA indicating that addition of MWNTs improves the thermal stability of PLA. The result is attributed to good thermal properties of the MWNTs and good interfacial interaction of MWNTs with the polymer matrix produced by the uniform MWNTs dispersion in the PLA, as shown in Fig. 1.

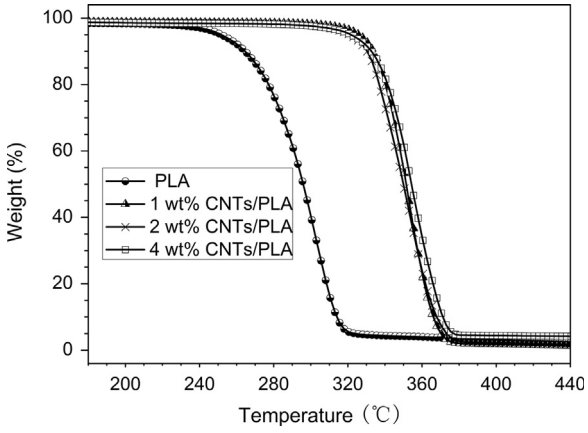

Fig. 2 Effect of carbon nanotubes on thermal stability of PLA nanocomposites.

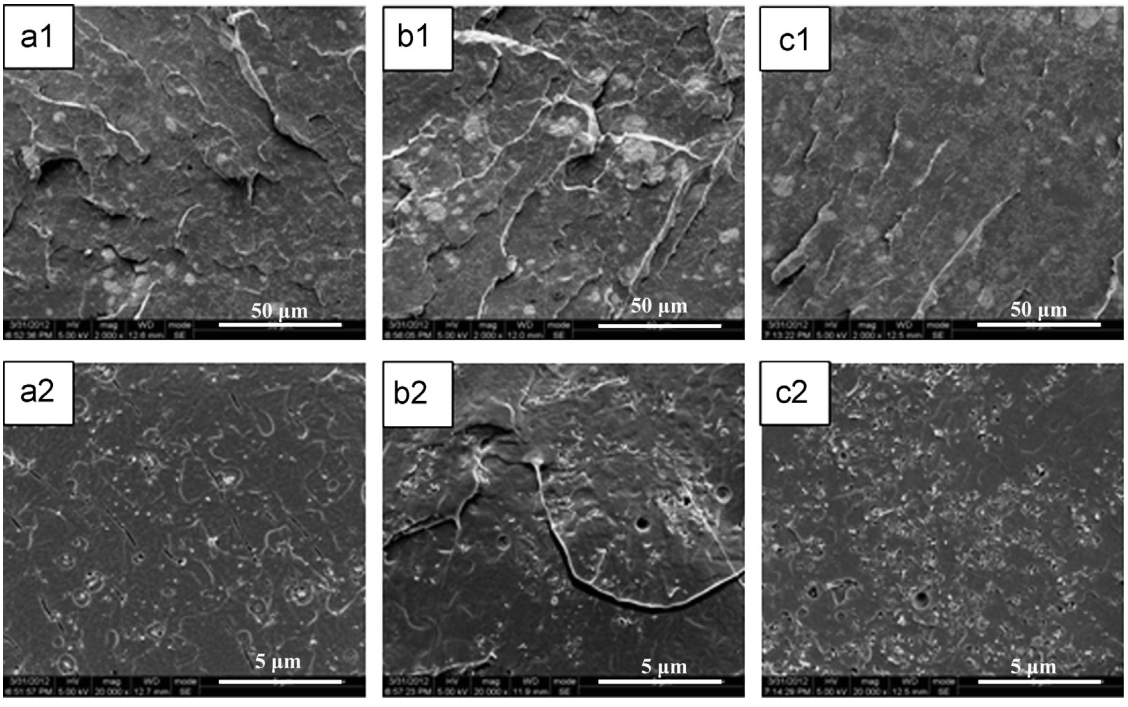

Fig. 1 SEM images of PLA/CNTs nanocomposites with different MWNTs content: (a_1) (a_2) 1 wt%, (b_1) (b_2) 2 wt%, (c_1) (c_2) 4 wt%. For (a_1) (b_1) and (c_1), the scale bar is 50 μm, and for (a_2) (b_2) and (c_2), the scale bar is 5 μm.

3.2. *The effect of saturation parameters on morphology of foams*

In order to obtain various cell structures of foams, the saturation temperature ranging from 109 °C to 121 °C and pressure ranging from 18 MPa to 26 MPa were used. The morphology of PLA/CNT4 foams affected by gas saturation parameters is shown in Fig. 3. The PLA/CNT4 foams saturated at 109 °C, 20 MPa and 115 °C, 18 MPa exhibit non-uniform morphology with nanometer scale cells (Fig. 3 (a) and (d)). Other foams have uniform and nearly spherical cells in micrometer scale (Fig. 3(b), (c) and (e), (f)).

The cell structure of foam is strongly affected by the rheological properties of materials and the gas saturation parameters [26]. The lower saturation pressure (18 MPa) and temperature (109 °C) lead to the higher viscosity which prevents cell growing and then results in smaller cells. On the other hand, as a semi-crystalline polymer, the crystallization behavior of PLA during saturated by $scCO_2$ can also influence the cell structure. The DSC curves of PLA/CNT4 nanocomposite and its foams are shown in Fig. 4 and the χ_c is listed in Table 1. The χ_c of foams saturated at 115 °C, 18 MPa and at 109 °C, 20 MPa was 23.6% and 27.1%, respectively. The higher χ_c of the two samples is mostly attributed to CO_2-induced crystallization during saturation and not from the strain-induced crystallization during foaming process discussed in

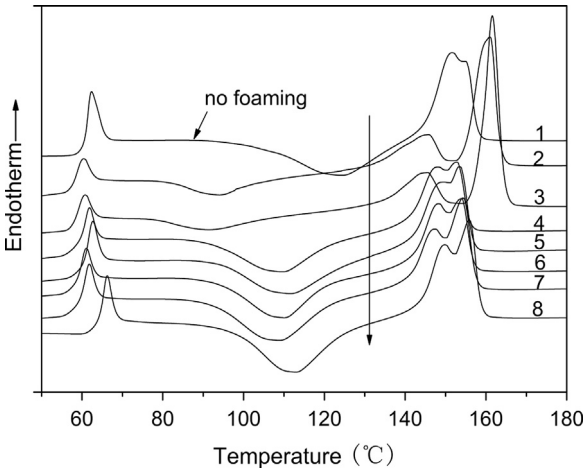

Fig. 4 DSC curves of the PLA/CNT4 nanocomposite and foams with different saturation conditions. The density decreases with the arrow direction. Curve 1 is for PLA/CNT4 nanocomposite and curves 2–8 are for PLA/CNT4 foams with different saturation conditions: 109 °C, 20 MPa, 115 °C, 18 MPa, 115 °C, 24 MPa, 121 °C, 20 MPa, 115 °C, 22 MPa, 115 °C, 20 MPa, 115 °C, 26 MPa.

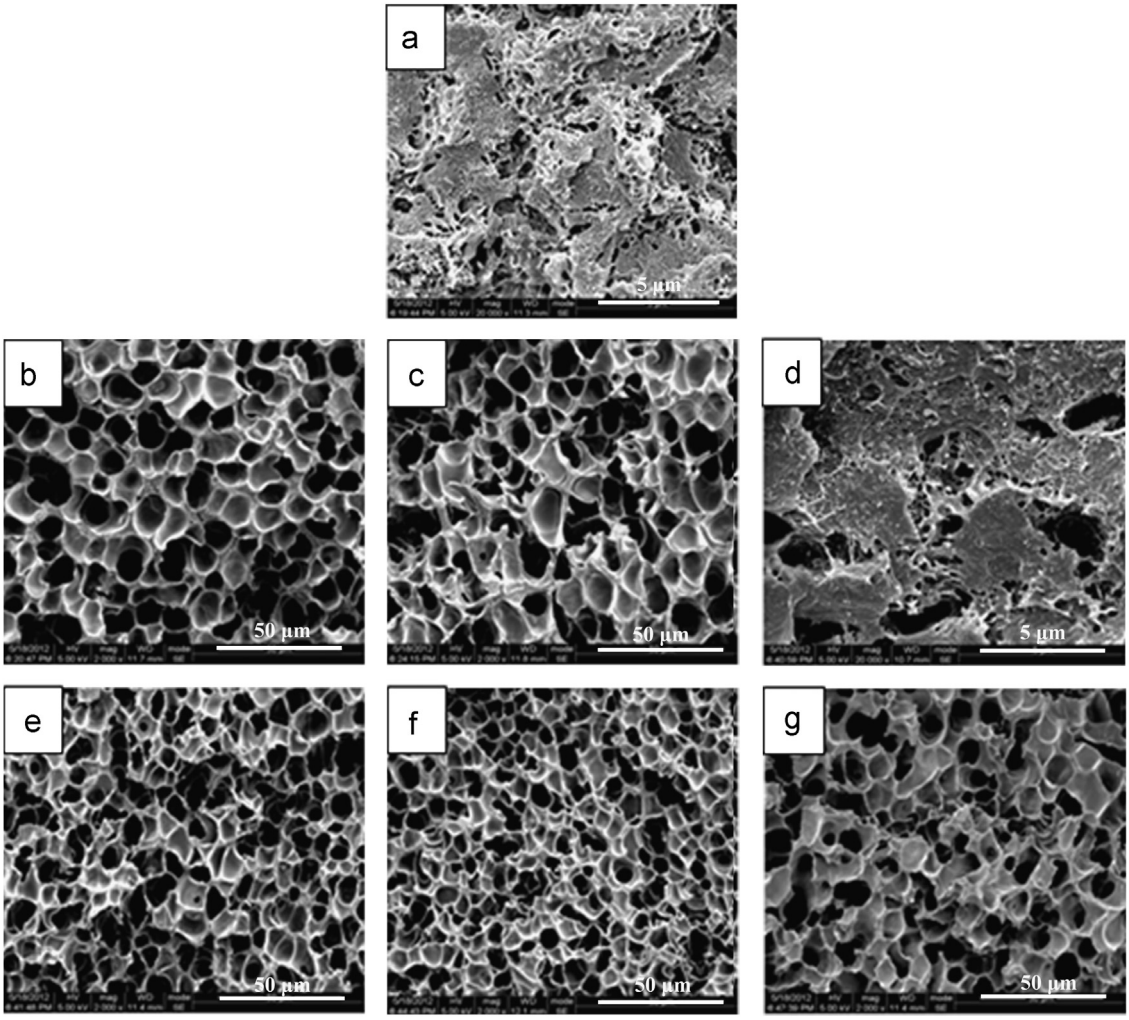

Fig. 3 SEM images of PLA/CNT4 foams obtained with different saturation conditions: (a) 109 °C, 20 MPa, (b) 115 °C, 20 MPa, (c) 121 °C, 20 MPa, (d) 115 °C, 18 MPa, (e) 115 °C, 22 MPa, (f) 115 °C, 24 MPa and (g) 115 °C, 26 MPa.

Table 1 Density, volume content of MWNTs, χ_c and volume resistivity of PLA/CNT4 nanocomposite and foams. The samples were numbered according to the decrease in the volume content of MWNTs.

Samples	Saturation condition		Density (g/cm^3)	Volume content (%)	χ_c (%)	Volume resistivity (10^3 Ω cm)
	T (°C)	P (MPa)				
1	no foaming		1.14	2.40	1.9	0.93
2	109	20	1.00	1.90	27.1	0.53
3	115	18	0.81	1.53	23.6	2.15
4	115	24	0.52	0.98	4.8	4.15
5	121	20	0.49	0.93	3.9	5.94
6	115	22	0.48	0.91	4.2	7.93
7	115	20	0.42	0.81	2.0	13.96
8	115	26	0.37	0.71	2.0	15.13

the later section. Liao et al. [27] reported the effect of crystallinity of PLA on foam morphology. Cell nucleation preferentially occurs at the interfaces between crystalline and amorphous regions due to the lower activation energy barrier required to overcome. Highly order crystalline structure enhances the polymer modulus which hinders cells growing. Therefore, cells with the high density and small size were achieved for foams saturated at 109 °C, 20 MPa and 115 °C, 18 MPa (Fig. 3(a) and (d)) which have high χ_c.

Since CO_2 does not dissolve in crystalline region, the nucleation is non-uniform which produces the non-uniform cell structure ultimately. However, at the higher saturation temperature including 115 °C and 121 °C and pressure ranging from 22 MPa to 26 MPa, low crystallinity less than 5% shown in Table 1 and the viscosity of polymer are proper for PLA/CNT4 to form nearly spherical and uniform cell structure.

The effects of saturation pressure on cell structure of foams have been studied at a constant saturation temperature of 105 °C. With the saturation pressure increasing from 20 MPa to 24 MPa, the average cell size of PLA/CNT4 foams decreases and the cell density increases (Fig. 3(b), (e) and (f)). The average cell size and cell density of foams are determined by the competition between cell nucleation and growth rates [28]. As the pressure increases, the supersaturation increases once depressurization is imposed which leads to nucleation rate dominating. Consequently, the higher saturation pressure generates more bubble nucleus and leads to a higher cell density and smaller cell sizes in obtained foams. However, when the saturation pressure increases to 26 MPa the average cell size of PLA/CNT4 foam increases and the cell density decreases (Fig. 3(g)). It is known that an increase in CO_2 saturation pressure tends to increase the solubility of CO_2 in polymer matrix. CO_2 can decrease the glass transition temperature (T_g) of polymer [29] and reduce polymer viscosity due to its plasticizing effect [30]. Thus both increasing the saturation temperature and pressure can lead to the decrease of the viscosity of polymer [31]. Increasing saturation pressure could amount to increasing saturation temperature. When the saturation pressure is high enough like 26 MPa, T_g and viscosity depression is high due to the much amount of CO_2 dissolved in the PLA. As a result, the larger cells are achieved (Fig. 3(g)).

3.3. *Thermal properties of PLA/CNT4 nanocomposite and foams*

DSC curves of the PLA/CNT4 nanocomposite and its foams with different saturation conditions are shown in Fig. 4. The exothermic peak and the endothermic peak exist in the DSC curves of all the samples. These exothermic and endothermic peaks are attributed to the cold crystallization and melting process of samples during the DSC heating run, respectively. The exothermic peak area of the PLA/CNT4 foams with saturated at 109 °C, 20 MPa and 115 °C, 18 MPa is much smaller than the endothermic peak area respectively. However, for other samples the area of the exothermic peak and the endothermic peak are approximately equal. We can get the degree of crystallinity of samples from the enthalpy of crystallization and melting and the degree of crystallinity (χ_c) of samples is shown in Table 1. The χ_c of PLA/CNT4 foams saturated at 109 °C, 20 MPa and 115 °C, 18 MPa is 27.1% and 23.6%, respectively. The χ_c of other foams is less than 5%.

CO_2-induced crystallization or strain-induced crystallization may lead to the crystallinity in foamed polymer [32]. It is known that strain-induced crystallization of polymer foam occurs with a biaxial extensional flow during cell growth. The more largely cell grows, the more strain-induced crystallization occurs. The PLA/CNT4 foam samples with saturated at 109 °C, 20 MPa and 115 °C, 18 MPa possess less biaxial extensional flow during cell growth because of the smaller cell sizes shown in Fig. 3, indicating that the most of crystallization of these foam samples probably occurred during the saturation in $scCO_2$.

The exothermic peaks of these two foam samples saturated at 109 °C, 20 MPa and 115 °C, 18 MPa around 95 °C and the exothermic peaks of other foam samples around 110 °C are lower than that of nanocomposite sample. That is to say, annealing of nanocomposites in $scCO_2$ quickens the cold crystallization process of PLA. The result is likely because the order crystalline structure of PLA becomes the nucleation point of the cold crystallization during DSC heating run.

3.4. *Electrical properties of foams*

Fig. 5 shows the volume resistivity versus the volume content of MWNTs for the PLA/CNT4 foams. The volume resistivity of the PLA/CNT4 foams decreases from 15.13×10^3 Ω cm to 0.53×10^3 Ω cm with the volume content of MWNTs increasing from 0.71% to 1.90%, as shown in Table 1. Compared with PLA/CNT4 nanocomposite which has the volume resistivity of 0.93×10^3 Ω cm, the volume resistivity of all the foams, except for sample 2 which was saturated at 109 °C, 20 MPa, increases slightly within 2 orders of magnitude. The expansion of nanocomposites by foaming results in the reduction of the density and the volume

content of MWNTs (shown in Table 1) and introduces the gaseous phase. The conductivity of the porous composites reduces since the conductivity of air is less than that of PLA/MWNTs. It is easily explained that the volume resistivity depends upon the volume content of MWNTs of PLA/CNT4 foams. However, the volume resistivity is not linearly related to the volume content of MWNTs. The result can be possibly explained by the morphology of the foam. As shown in Fig. 6, the PLA/MWNTs foam is composed of three phases including PLA matrix, carbon nanotube fillers and gaseous phase. The MWNTs disperse in the wall of cell and form an interconnected carbon nanotubes network which builds electrical conduction pathways. As shown in Fig. 6, the thickness of the cell wall is not consistent and some walls are broken which form the open cell structure. The MWNTs content in the wall decreases when the thickness of the cell wall decreases which reduces the conductivity of cell wall. Further on, when the thickness of cell wall is too thin, no MWNTs are in the wall leading to a transition from three-dimensional (3D) to two-dimensional (2D) percolation which increases the percolation and decreases the conductivity of the wall [19]. Li et al. [19] have reported that the conductivity of PU/CNT foams depended on the thickness of the cell wall. Moreover, the open cell structure also decreases the conductivity of foam because the conductive pathways are broken.

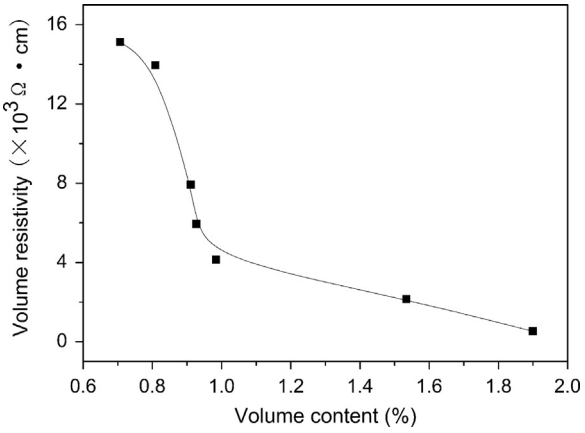

Fig. 5 The volume resistivity of the PLA/CNT4 foams versus the volume content of MWNTs.

The volume resistivity of PLA/CNT4 foam saturated at 109 °C, 20 MPa is slightly less than that of the PLA/CNT4 nanocomposite. The result possibly can be explained by the MWNTs structural change due to the crystallization of PLA. Jeon et al. [33] reported that the conductivity of polypropylene/polyethylene/single walled carbon nanotube (PP/PE/SWCNT) composites increased with increasing crystallinity due to the SWCNT structural change in which the SWCNT was less curled and more connected. For PLA/CNT foams, the conductivity is affected by two factors oppositely that is crystallization of PLA increases conductivity and foaming decreases conductivity. Because of the lower expansion ratio and the higher crystallinity, the volume resistivity of PLA/CNT4 foam saturated at 109 °C, 20 MPa is slightly lower than that of the PLA/CNT4 nanocomposite.

4. Conclusions

PLA/MWNTs nanocomposites were prepared by solution blending. SEM analysis reveals that MWNTs were well dispersed in PLA matrix. Thermal properties of the nanocomposites were investigated by TGA analysis. It was found that the introduction of MWNTs to PLA resulted in significant improvement of the decomposition temperature of PLA. Electric conductive PLA/CNT foams were produced via a pressure-quench process using $scCO_2$ as the blowing agent. The morphology study shows that the nanometer-scale cellular structure formed when the saturation pressure and temperature were 109 °C, 20 MPa and 115 °C, 18 MPa due to the higher crystallinity and viscosity. The micrometer-scale open cellular structure developed at appropriate saturation condition due to the lower crystallinity and proper viscosity. The PLA/CNT nanocomposites foams fabricated in this study were found to have low volume resistivity from 0.53×10^3 Ω cm to 15.13×10^3 Ω cm which depended on the volume content of MWNTs in the foams. The volume resistivity of PLA/CNTs foams was affected by cell structure and crystallization of foams oppositely. Foaming reduced the electrical conductivity of the nanocomposite due to the decrease of volume content of MWNTs and the break of conductive pathways, while crystallization of PLA in CO_2 increased the electrical conductivity possibly because

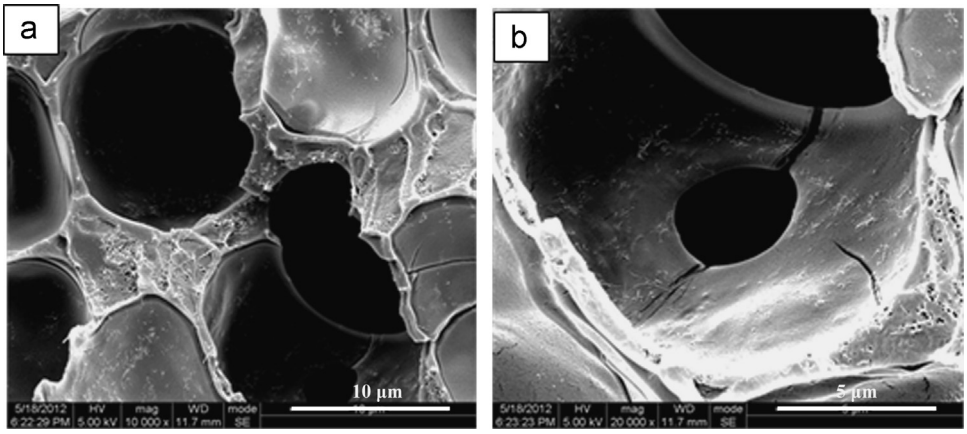

Fig. 6 SEM images of PLA/CNT4 foam obtained with the saturated parameters of 121 °C, 20 MPa, (a) low magnification and (b) high magnification.

MWNTs were less curled and more connected in crystalline samples.

Acknowledgments

This work is supported by National Natural Science Foundation of China (Nos. 51103091 and 51121001), Scientific Research Foundation for the Returned Overseas Chinese Scholars (No. 20101174-4-3) from the State Education Ministry, and Chengdu City Bureau of Technology, China (No. 11DXYB336JH).

References

[1] L. Yu, K. Dean, L. Li, Progress in Polymer Science 31 (2006) 576–602.
[2] J.M. Zhang, Y.X. Duan, A.J. Domb, et al., Macromolecules 43 (2010) 4240–4246.
[3] X. Liao, A.V. Nawaby, P. Whitfield, et al., Biomacromolecules 7 (2006) 2937–2941.
[4] T. Chang, Applied Mechanics and Materials 52–54 (2011) 2145–2150.
[5] H.C. Chen, C.H. Tsai, M.C. Yang, Journal of Polymer Research 18 (2011) 319–327.
[6] A.J. Svagan, A. Akesson, M. Cárdenas, et al., Biomacromolecules 13 (2012) 397–405.
[7] J. Joo, C.Y. Lee, Journal of Applied Physics 88 (2000) 513–518.
[8] X.P. Shui, D.D.L. Chung, Journal of Materials Science 35 (2000) 1773–1785.
[9] J.H. Wu, D.D.L. Chung, Carbon 41 (2003) 1313–1315.
[10] P. Annadurai, A.K. Mallick, D.K. Tripathy, Journal of Applied Polymer Science 83 (2002) 145–150.
[11] M. Paligová, J. Vilčáková, P. Sáha, et al., Physica A 335 (2004) 421–429.
[12] Y.L. Yang, M.C. Gupta, K.L. Dudley, et al., Nano Letters 5 (2005) 2131–2134.
[13] Z. Spitalsky, D. Tasis, K. Papagelis, et al., Progress in Polymer Science 35 (2010) 357–401.
[14] C. Peng, S.W. Zhang, D. Jewell, et al., Progress in Natural Science 18 (2008) 777–788.
[15] R. Ramasubramaniam, J. Chen, H.Y. Liu, Applied Physics Letters 83 (2003) 2928–2930.
[16] Y. Yang, M.C. Gupta, K.L. Dudley, et al., Nanotechnology 15 (2004) 1545–1548.
[17] H.J. Barraza, F. Pompeo, E.A. O'Rear, et al., Nano Letters 2 (2002) 797–802.
[18] H.M. Kim, K. Kim, C.Y. Lee, et al., Applied Physics Letters 84 (2004) 589–591.
[19] X.B. Xu, Z.M. Li, L. Shi, et al., Small 3 (2007) 408–411.
[20] C.B. Park, D.F. Baldwin, N.P. Suh, Polymer Engineering and Science 35 (1995) 432–440.
[21] S. Pilla, A. Kramschuster, S. Gong, et al., International Polymer Processing 22 (2007) 418–428.
[22] R. Rizvi, O. Khan, H.E. Naguib, Polymer Engineering and Science 51 (2011) 43–53.
[23] S.K. Goel, E.J. Beckman, Polymer Engineering and Science 34 (1994) 1137–1147.
[24] Y.L. Li, Y. Wang, L. Liu, et al., Journal of Polymer Science Part B: Polymer Physics 47 (2009) 326–339.
[25] E.W. Fischer, H.J. Sterzel, G. Wegner, Kolloid-Zeitschrift und Zeitschrift für Polymere 251 (1973) 980–990.
[26] R.G. Liao, W. Yu, C.X. Zhou, Polymer 51 (2010) 568–580.
[27] X. Liao, A.V. Nawaby, P.S. Whitfield, Polymer International 59 (2010) 1709–1718.
[28] S. Cotugno, E.D. Maio, G. Mensitieri, et al., Industrial and Engineering Chemistry Research 44 (2005) 1795–1803.
[29] X. Liao, J.S. He, J. Yu, Polymer 46 (2005) 5789–5796.
[30] Z.Y. Zhang, Y.P. Handa, Macromolecules 30 (1997) 8505–8507.
[31] Z.M. Xu, X.L. Jiang, T. Liu, et al., Journal of Supercritical Fluids 41 (2007) 299–310.
[32] W.T. Zhai, Y. Ko, W.L. Zhu, et al., International Journal of Molecular Sciences 10 (2009) 5381–5397.
[33] K. Jeon, S. Warnock, C. Ruiz-Orta, et al., Journal of Polymer Science Part B: Polymer Physics 48 (2010) 2084–2096.